Check for updates

Anatase TiO$_{2-x}$ and zwitterionic porphyrin polymer-based nanocomposite for enhanced cancer photodynamic therapy†

Jiaxu Li, [ID] [a] Dengshuai Wei*[b] and Qinrui Fu [ID] *[c]

Photodynamic therapy has been used as a treatment option for cancer; however, the existing TiO$_2$ photosensitizer does not have the ability to specifically target cancer cells. This lack of selectivity reduces its effectiveness in overcoming cancer resistance. To improve photodynamic therapy outcomes, an innovative solution is proposed. In this study, we report on the compounding of a zwitterionic covalent organic polymer (COP) with a TiO$_2$ photosensitizer for the first time. The aim is to overcome cancer cellular resistance. A one-pot synthetic strategy, which includes the construction of a porphyrin-based COP has been employed. This strategy has also been applied to the rapid preparation of anatase defective TiO$_2$ (TiO$_{2-x}$). To improve the hydrophilic and antifouling properties of the polymer, zwitterion L-cysteine has been conjugated with a porphyrin-based COP using a thiol–ene "click chemistry" reaction. The novel zwitterionic porphyrin-based COP has the ability to trigger biodegradation under the acid microenvironment due to the presence of acid-sensitive β-thioether esters. When combined with TiO$_{2-x}$, the resultant nanocomposite produces an enhanced photodynamic therapy effect for drug-resistant cancer cells under NIR laser irradiation. This is due to the strong mutual sensitization of zwitterionic porphyrin-based COP and TiO$_{2-x}$. Importantly, the nanocomposite delivery system exhibits excellent cytocompatibility in the dark and has the potential to improve the accuracy of cancer diagnosis through fluorescence imaging. The results of this study demonstrate the potential application of this alternative nanocomposite delivery system for remote-controllable photodynamic therapy of tumors.

1. Introduction

Over the past few decades, cancer has been one of the most life-threatening diseases in the world. To treat this disease, great efforts have been made.[1–3] However, cancer resistance such as chemotherapy resistance can undermine the efficacy of cancer therapies.[4] Photodynamic therapy (PDT) as a cancer treatment with specificity and non-invasiveness has been introduced into clinical trials to improve the anti-cancer effect by overcoming multidrug resistance,[5–7] with reduced side effects, such as physical and mental pain.[8]

Recently, nanoscale covalent organic polymers (COPs) or covalent–organic frameworks (COFs) with well-defined cross-linked polymeric network structures and repeated organic unit compositions have attracted great attention as potential nanomedicine platforms.[9] Various nano-COPs and nano-COFs with large surface areas and porous structures have been utilized as a new class of drug carriers for efficient drug loading.[10–12] By rational selection of the organic building blocks, such as photosensitive porphyrin, novel nano-COFs and nano-COPs with different chemical and physical properties and functionalities can be formulated to enable cancer theranostic applications.[13–16] However, without further modifications, most of these as-synthesized COPs or COFs cannot be directly injected intravenously for *in vivo* use because of their limited hydrophilicity and dispersibility.[17] The combination of water-soluble polyethylene glycol and zwitterion groups to modify the COPs or COFs can improve the hydrophilicity and provide antifouling properties, as there is a strong hydration layer formed on the surface of zwitterionic polymers which increases the distances between biomolecules and the surface.[2,18] Through artful means, it can efficiently increase

[a] Guangxi Key Laboratory of Natural Polymer Chemistry and Physics, College of Chemistry and Materials, Graduate School, Nanning Normal University, Nanning 530001, People's Republic of China
[b] Department of Pharmaceutics, School of Pharmacy, Qingdao University, Qingdao 266021, People's Republic of China. E-mail: weidengshuai@163.com
[c] Institute for Translational Medicine, College of Medicine, Qingdao University, Qingdao 266021, People's Republic of China. E-mail: fuqinrui2022@qdu.edu.cn
†Electronic supplementary information (ESI) available. See DOI: https://doi.org/10.1039/d3nr03012a

the hydrophilicity and functionality of COPs, such as using the synthon fumaryl chloride with the high reaction (the chloride group) and functionalized reaction site (C=C bond) for copolymerization and the thiol–ene "click chemistry" reaction.

Moreover, as one of the most widely used semiconductor photocatalysts, pristine TiO_2 particles can be used as promising PDT photosensitizers, and have shown great potential in the phototherapy of malignant cells due to their excellent photostability and irradiation-induced phototoxicity by ultraviolet light (200–400 nm).[19] TiO_2 is non-toxic and chemically stable, and it has a wide band gap energy (3.2 eV for anatase and 3 eV for rutile).[20] When TiO_2 is irradiated with ultraviolet light, electrons in its valence band will be excited into the conduction band, forming highly active negatively charged electrons e^-, and at the same time forming positively charged holes h^+ in the valence band, that is, electron–hole pairs. The main crystal types of TiO_2 are the rutile type and anatase type. Compared with rutile TiO_2, anatase TiO_2 has the smallest relative density (3.8–3.9 g cm^{-3}). Anatase TiO_2 is mostly used in textile and chemical fiber industries, and its hydrophilic and hygroscopic properties are stronger than those of rutile TiO_2.[21] Moreover, anatase TiO_2 is popular in solar cell applications due to its high electron mobility, low dielectric constant and low density.[22] As a photocatalyst, nano-anatase TiO_2 can make full use of light energy, which is not only efficient, but also environmentally friendly. In addition, nano-anatase TiO_2 shows good photostability and high reactivity during the catalytic reaction, which is a kind of nano-functional material that has the broadest application prospect recently. It is widely used in wastewater treatment, air purification, sterilization, medical technology and the preparation of environmentally friendly material fields.[23]

In order to broaden the application conditions of anatase TiO_2 and eliminate the harm of ultraviolet light to the human body during the treatment, many efforts have been made to improve the anatase TiO_2 photoelectric conversion efficiency by decreasing the rapid combination of photo-generated electrons and holes, which leads to the formation of ROSs and inducing toxicity to cancer cells,[24,25] and search the effective methods to obtain modified anatase TiO_2 for visible light (400–700 nm) or NIR (700–1700 nm) induced PDT.[25–28] Compared with the complicated synthesis or doping of metallic elements with anatase TiO_2, the preparation of black anatase defective TiO_2 (termed TiO_{2-x}) nanocrystals to improve photoactivity and widen their optical response region to NIR may be a more direct, efficient and low-cost strategy.[29] The black anatase TiO_{2-x} nanocrystals could improve long wavelength absorption for deeper penetration and suppress electron–hole pair recombination for higher PDT efficacy. It is of great importance to find an appropriate method to improve
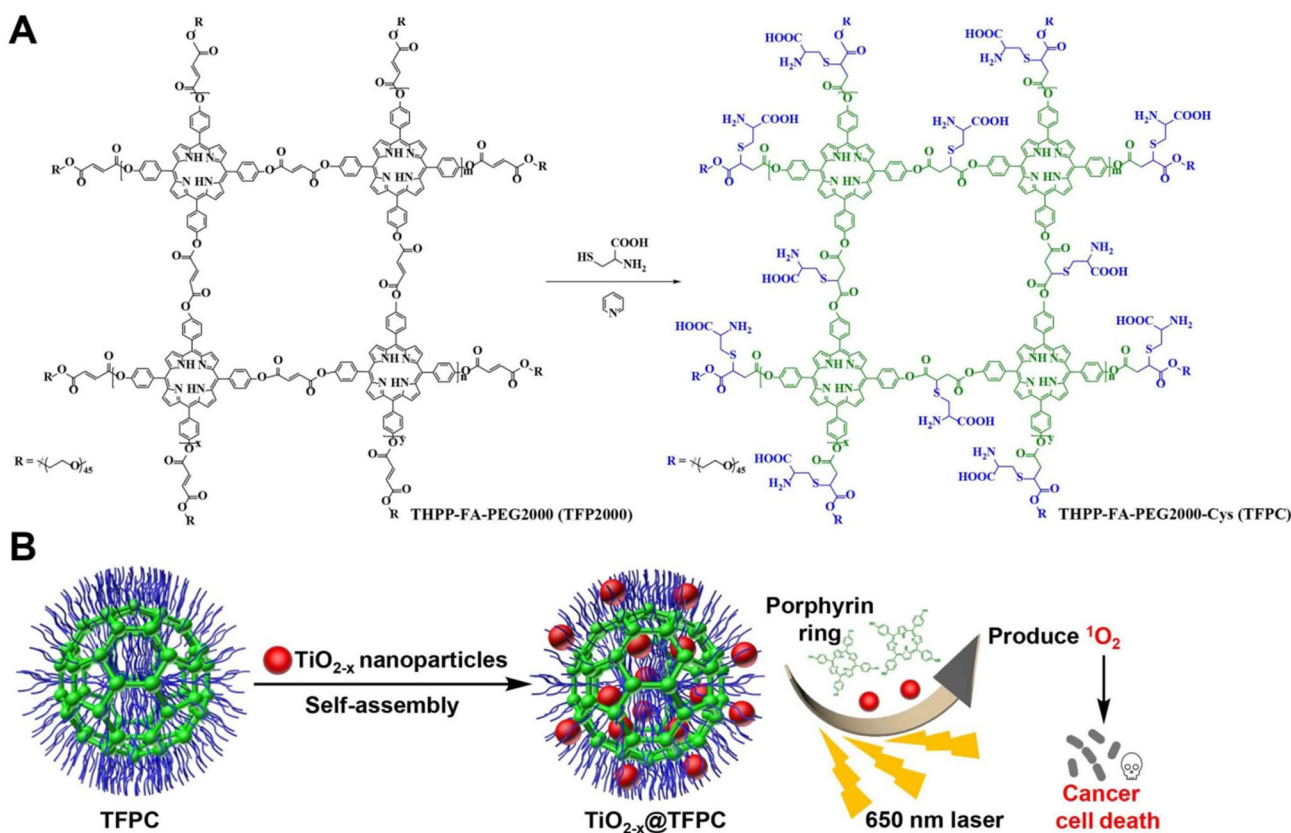
Scheme 1 Design of (A) the zwitterionic porphyrin-based covalent organic polymer TFPC and (B) combined with the photosensitizer TiO_{2-x}, the structure of the enhanced photodynamic therapy nanocomposite TiO_{2-x}@TFPC for treating the drug-resistant cancer cells.

the specific binding of TiO_{2-x} nanoparticles with cancer cells, to construct a localized enhanced PDT system in the field of medical nanotechnology, especially overcoming cancer resistance to cancer therapy.

Hence, herein, we developed an enhanced cancer photodynamic therapy nanocomposite based on a porphyrin-based COP (termed TFP2000), amino acid type zwitterion L-cysteine and black anatase TiO_{2-x} (Scheme 1). To the best of our knowledge, this is the first time the use of COPs to load TiO_2 as a therapeutic nano-system for enhanced cancer photodynamic therapy is reported. First, the polyester TFP2000 was synthesized *via* a one-pot esterification from the *meso*-5,10,15,20-tetra(4-hydroxylphenyl)porphyrin (THPP), fumaryl chloride and methoxy polyethylene glycols. Then, the zwitterion L-cysteine was successfully conjugated to TFP2000 using a thiol–ene "click chemistry" reaction (Scheme 1A). Meanwhile, tetrabutyl titanate was mixed with diethylene glycol (DEG) by stirring to form a titanium glycolate gel.[29] Glycosylation can increase the stability of black TiO_2 nanoparticles in a physiological environment, which is beneficial for the high anticancer effect *in vitro* and *in vivo*.[30] Then water was added to facilitate sufficient hydroxylation, since excess hydroxylation can direct towards black TiO_2.[31] In addition, aqueous mediated reactions lead to crystal phase formation at relatively low calcination temperatures.[32] After high-temperature calcination and rapid cooling to room temperature, the formed hydrated titanium glycolate gel sample can produce TiO_{2-x} (shown in Fig. 2A). Finally, the hydrophobic oxygen vacancy rich black anatase TiO_{2-x} loads into TFPC to form nanocomposites for enhanced cancer photodynamic therapy (Scheme 1B).

2. Results and discussion

2.1 Structure and properties of the photosensitizer TFPC

The obtained TFP2000 was characterized by ^1H NMR (Fig. S1A†). The peaks at 7.14–8.95 ppm are attributed to the protons of THPP. The peaks at 3.40–3.69 ppm and 6.70–6.78 ppm are ascribed to the protons of PEG and ">HC=CH<" in the fumaryl group, respectively. These results indicate the successful formation of TFP2000. TFP2000 was further characterized by FT-IR, and the band of C=O stretching vibrations in the >C=C–COOR ester group appears at 1724.46 cm^{-1} (Fig. S1B†). This relatively low wave number of the C=O band is due to conjugation with C=C. While in the infrared spectra of the zwitterionic copolyester TFPC, the band of C=O strong stretching vibrations of the ester group appears at 1754.48 cm^{-1}. These are consistent with the results reported in our previous work,[2] indicating that the zwitterionic COP TFPC is successfully synthesized. THPP, TFP2000 and TFPC ethanol dispersion solutions all showed typical absorbance peaked at 419 nm as measured using a UV-visible spectrometer (Fig. 1A and S2†). Moreover, TFPC only showed a small peak at around 650 nm and a negligible absorbance in the near infrared region (700–900 nm), which would not induce an obvious
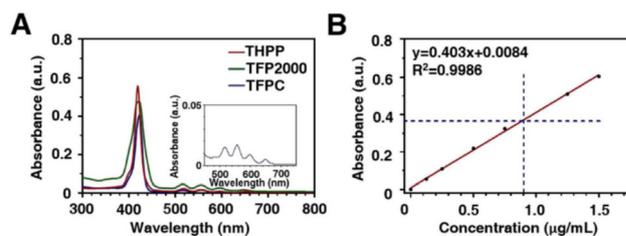

Fig. 1 (A) UV-vis spectra of free THPP (1.0 μg mL^{-1}), TFP2000 (200.0 μg mL^{-1}), and TFPC (50.0 μg mL^{-1}) in ethanol solution. (B) Normalized absorbance of THPP ethanol solution at varying concentrations (detected at 419 nm). The dashed lines mean the THPP porphyrin portion concentrations calculated from the standard curve with the detected UV absorption values of TFPC ethanol solution.

photothermal effect upon exposure to a 650 nm laser at 300 mW (the parameter used for following the PDT experiment), or a 630 nm laser at 50 mW cm^{-2} (the typical parameter for photothermal tumor therapy). The weight percentage of the THPP porphyrin portion within COP TFPC was detected to be 1.79% (Table S1†).

2.2 Structure and properties of the photosensitizer TiO_{2-x}

The obtained TiO_{2-x} was characterized by XPS (Fig. 2B). The $2p_{3/2}$ and $2p_{1/2}$ peaks of TiO_{2-x} are located at 458.7 and 464.6 eV, respectively (Fig. 2C). The sharp peak at 458.7 eV indicates the presence of a high concentration of Ti^{4+}.[34] In the O 1s XPS spectrum, the Ti–O–Ti peak is observed at 530.0 eV (Fig. 2D). This value is consistent with the earlier reported ones, which is attributed to the existing enormous oxygen vacancies produced during the hydrothermal process.[35,36] The calculated value of Δbinding energy (BE) = BE(O 1s) − BE(Ti $2p_{3/2}$) = 530.0 − 458.7 = 71.3 eV is in close proximity to that of anatase (~71.4 eV), also indicating clearly the domination of the Ti^{4+} state in the synthesized TiO_{2-x} powder.[34] During the preparation of TiO_{2-x}, tetrabutyl titanate and DEG are mixed homogeneously at the molecular level, to form Ti glycolate complexes and eliminate the possible bulk diffusion restriction during anatase phase formation. The peaks at 531.7 and 533.3 eV in O 1s XPS spectra confirm the presence of Ti–OH and free –OH species, respectively.[37] Sufficient hydroxylation can lead to the formation of black TiO_{2-x} and enhance visible light absorption substantially.[31,38] The valence band (VB) maximum of TiO_{2-x} is at 2.64 eV and the notable band tailing is at 0.43 eV as observed from VB XPS (Fig. 2E), suggesting the existence of a highly defective surface structure on TiO_{2-x}.[38,39] Rapid cooling after the high-temperature calcination reaction of generating TiO_{2-x} can assist in the formation of defect-rich nanocrystalline structures.[40]

The black anatase TiO_{2-x} was further characterised by UV-visible spectroscopy (Fig. 2F). Evidently, wide area absorption at around 900 nm (NIR region) can be observed. The corresponding band gap energy was calculated to be 1.78 eV using the Tauc plot (Fig. 2G), which is much lower than the wide band gap energy (3.2 eV for anatase)[42] of the colourless/white
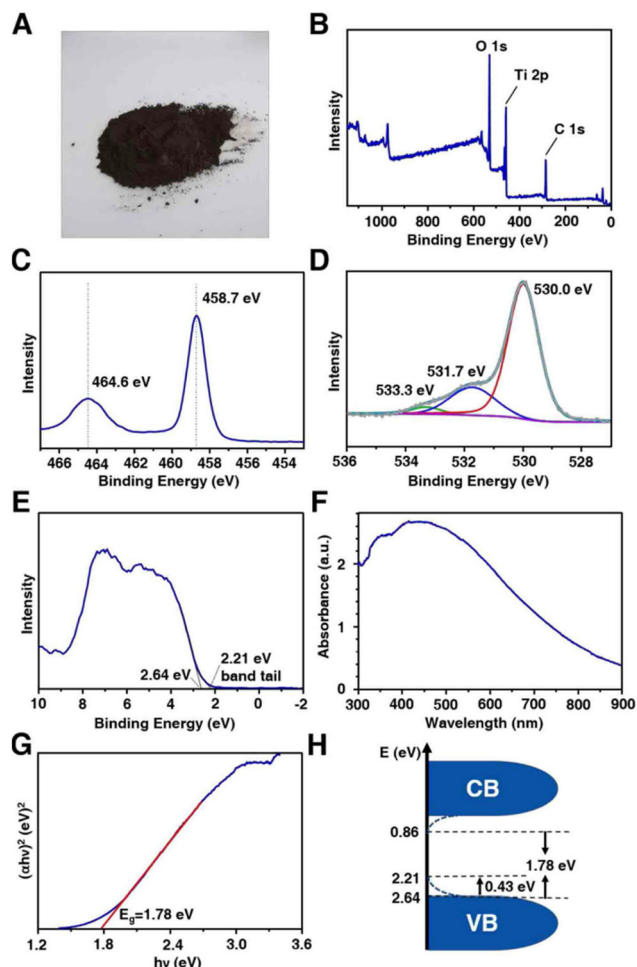
Fig. 2 (A) Digital image of the appearance of "black" anatase TiO_{2-x}. (B) XPS survey spectra of "black" anatase TiO_{2-x}. (C) Ti 2p XPS spectra. (D) O 1s XPS spectra. (E) VB XPS spectra. The thin black line indicates the location of the VB maximum. (F) UV-visible absorption spectra and (G) Tauc plot of "black" anatase TiO_{2-x}. (H) Density of states (DOS) of "black" anatase TiO_{2-x}.

Fig. 3 (A) XRD patterns, (B) TEM, (C) HRTEM images, and (D) SAED pattern of "black" anatase TiO_{2-x}. In (C), black short-dashed curves are applied to outline portions of the interface between the crystalline core and the disordered outer layer (marked by white arrows).

nature TiO_2. This substantial decrement in band gap energy, which leads to rapid photo-excitation of electrons from the VB to the conduction band (CB), can efficiently enhance the rate of generating reactive oxygen species (ROS) (*e.g.*, singlet oxygen ($^1O_2$)). Therefore, the density of states (DOS) diagram of black anatase TiO_{2-x} can be drawn (Fig. 2H), which shows that the narrowed band gap energy of black anatase TiO_{2-x} is due to the presence of mid-gap band states between the VB and the CB.[39] The main absorption onset and the VB edge of black anatase TiO_{2-x} are located at 2.64 eV and 2.21 eV, respectively. The maximum energy associated with the band tail blue-shifted, resulting in the VB maximum at 2.21 eV. Moreover, there may be CB tail states arising from disorders that extend below the CB minimum. Since the band gap of black anatase TiO_{2-x} from the optical absorption spectrum is 1.78 eV, the CB minimum would occur at 0.86 eV.[38,43] The VB maximum and CB minimum of mid-gap band states are mainly due to O 2p and Ti 3d orbitals, respectively.
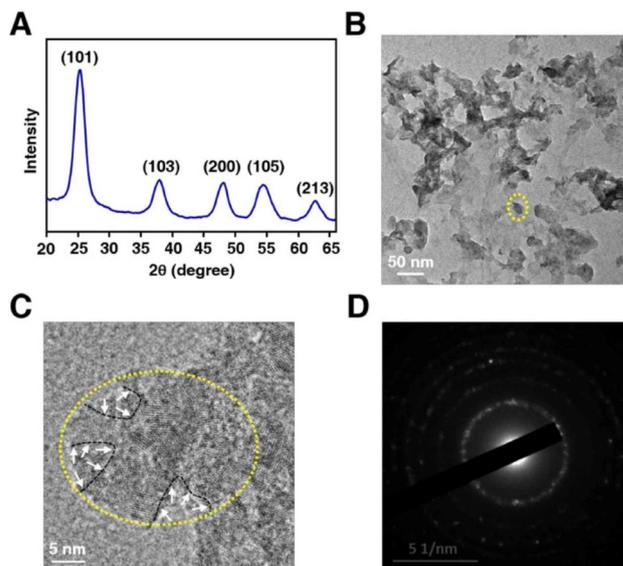
Furthermore, the XRD pattern of the black TiO_{2-x} shows peaks at 25.2°, 38.1°, 48.0°, 54.7° and 62.8° (Fig. 3A), corresponding to the (101), (103), (200), (105) and (213) lattice plane reflections of the anatase phase of TiO_2 (JCPDS 75-1537). The wide XRD peaks indicate that the average crystallite size of black TiO_{2-x} is small, and it was found to be 4.5 nm which corresponds to the main XRD peak along the (101) plane. A distorted spherical morphology of anatase TiO_{2-x} is observed from TEM analysis (outlined by a yellow dashed circle in Fig. 3B). The size of a single black TiO_{2-x} nanoparticle was measured around 23 nm, which is consistent with the result reported in the literature.[29] The surface defects and the lattice fringes (the lattice spacing is 0.35 nm) of TiO_{2-x} are evident in a certain area of the particle (outlined by a yellow dashed circle in Fig. 3C), and the lattice fringes fade out in a large area highlighted in the HRTEM image. The loss of lattice fringes also demonstrates that the defect states are present on the black anatase TiO_{2-x} surface.[41] The SAED pattern of black anatase TiO_{2-x} nanocrystals is shown in Fig. 3D. Therefore, the black anatase TiO_{2-x} is successfully prepared, and its structural characterization is clear.

2.3 Nanocomposites of the photosensitizers TFPC and black anatase TiO_{2-x}

The size and polydispersity index (PDI) of TFP2000 and TFPC nanoparticles and the TiO_{2-x}@TFPC nanocomposite in aqueous solution were characterized by DLS (Fig. 4A and S3†). The results demonstrate that there was a negligible change in the size when the zwitterion L-cysteine was introduced into TFP2000 to obtain TFPC (Table 1). However, the PDIs of these nanoparticles decreased in the system with moderate dis-
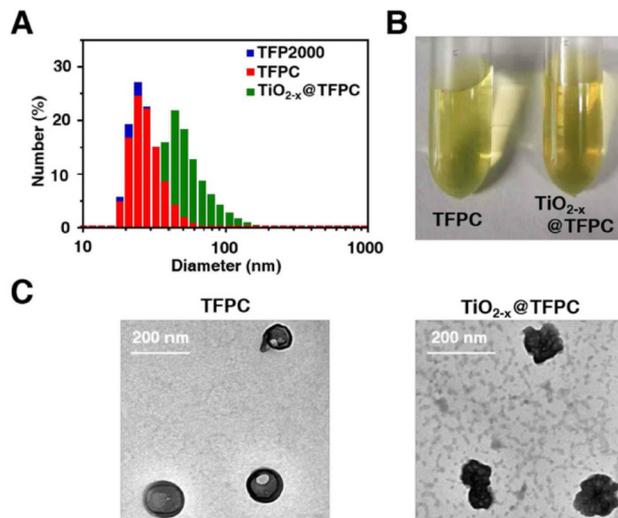
Fig. 4 Chemophysical characterization of the TFPC nanoparticles and TiO$_{2-x}$@TFPC nanocomposites. (A) Hydrodynamic diameter. (B) Digital images of TFPC nanoparticles (0.4 mg mL^{-1}) and TiO$_{2-x}$@TFPC nanocomposites (3 mg mL^{-1}) aqueous solution. (C) TEM.

Table 1 The summary of the size data and Ti concentrations of the nanoparticles or nanocomposites

Sample	d_{DLS}/nm	PDI	Ti concentration [µg mL^{-1}]
TFP2000	49.6 ± 1.0	0.367 ± 0.015	—
TFPC	51.7 ± 0.5	0.206 ± 0.019	—
TiO$_{2-x}$@TFPC	173.4 ± 0.5	0.166 ± 0.018	4.59

persion, indicating that the introduced hydrophilic zwitterion L-cysteine makes the particle size more uniform. The size and PDI of the TiO$_{2-x}$@TFPC nanocomposite were 173.4 ± 0.5 nm and 0.166 ± 0.018, respectively. In a previous report, the polycarboxylate ethers can develop hydrogen bridging bonds between their carboxylic groups and the hydroxyl groups on the TiO$_2$ nanoparticle surface, and can also act as a surfactant to sterically stabilize the TiO$_2$ nanoparticles *via* their bulky polyethylene oxide side chains.[44] The efficiency of polycarboxylate ethers as stabilisers mainly depends on their anchoring strength onto the particles, the particle surface coverage and the polymer composition (*e.g.*, chain length). Similarly, the presence of long polyethylene oxide side chains (2000 g mol^{-1}) on TFPC nanoparticles can provide strong steric stabilisation for compounding TiO$_{2-x}$ nanoparticles, and the parts of undeprotonated –COOH on the TFPC nanoparticles' cysteine moiety can also anchor the TiO$_{2-x}$ nanoparticles by hydrogen bridging bonds.[45] During the simple preparation process of the TiO$_{2-x}$@TFPC nanocomposite, TiO$_{2-x}$ was compounded to COP TFPC by stirring, and the obtained dialysis aqueous solution was centrifuged to remove the large aggregates, and thus the size of the final TiO$_{2-x}$@TFPC nanocomposites increases about 2.35 times that of TFPC. The PDI of the TiO$_{2-x}$@TFPC nanocomposites is small, implying a relatively narrow size dis-

tribution. The COP TFPC nanoparticles and TiO$_{2-x}$@TFPC nanocomposites showed excellent solubility in water benefitting from the presence of PEG and zwitterion L-cysteine (Fig. 4B). TEM micrographs revealed that these particles exist in a non-aggregated state (Fig. 4C).

The size data and zeta potential change of TFPC and TiO$_{2-x}$@TFPC detected by DLS are shown in Fig. S4† to study the stability and zeta potential of the nanoparticles in pH 7.4 buffer solution. There was no evident change in the size and PDI of TFPC nanoparticles and TiO$_{2-x}$@TFPC nanocomposites, indicating that these nano-systems were stable enough. The zwitterionic porphyrin-based covalent organic polymer TFPC and its contained TiO$_2$ composite TiO$_{2-x}$@TFPC are the nanoparticles and nanocomposites with zeta potentials of −16.31 and −22.84 mV, respectively. The zeta potentials of these nano-systems with charge can remain stable with little change in PBS buffer solutions at pH 7.4 within 6 days (Fig. S4†). The presence of the neutral zwitterionic cysteine moiety attached to the PEG-containing polyester chain tends to shift the zeta potential toward neutrality (~−10 mV) as expected, due to a shielding of the polyester core surface charges by the PEG and zwitterion layer.[46,47] The negative charge with zeta potentials may be due to the mild deprotonation of –COOH on the cysteine moiety at pH > 7 as the isoelectric point of L-cysteine is 5.05. The previous literature also reported that the degree of formation of negatively charged L-cysteine species is nearly 90% at pH > 7.[45] When the TFPC nanoparticles compounded with TiO$_{2-x}$ nanoparticles through the strong steric stabilisation of long polyethylene oxide side chains (2000 g mol^{-1}) on TFPC nanoparticles, the shielding effect of the polyester core surface charges by the PEG layer was strengthened. Therefore, the zeta potential absolute value of TiO$_{2-x}$@TFPC nanocomposites is higher than that of TFPC nanoparticles. These data show that the TFPC nanoparticles and TiO$_{2-x}$@TFPC nanocomposites are suitable for subsequent correlative photodynamic therapy of cancer cell experiments.

Furthermore, the Ti concentration of the successfully prepared TiO$_{2-x}$@TFPC nanocomposite aqueous solution was found to be 4.59 µg mL^{-1} using ICP-MS (Table 1). The thermogravimetric analysis curves of the lyophilized nanoparticles and nanocomposites show that the temperatures at the maximum mass loss rate of TFPC and TiO$_{2-x}$@TFPC are 405.02 °C and 417.73 °C, respectively (Fig. S5†). When the organic part of the TFPC nanoparticles burns out completely to 543 °C, the residual contains the Ti of TiO$_{2-x}$@TFPC, whose content is 6.56% and is consistent with the result obtained by ICP-MS. SEM analysis characterizes the surface morphologies of lyophilized TiO$_{2-x}$@TFPC powders and the TiO$_{2-x}$@TFPC nanocomposites prepared by aqueous solution (Fig. S6†). It is also consistent with the result of TEM analysis (Fig. 4C).

2.4 Drug release and release mechanism of TiO$_{2-x}$@TFPC nanocomposites

The drug release profiles of the TiO$_{2-x}$@TFPC nanocomposites were detected over 48 h (Fig. 5A). When the nanocomposites
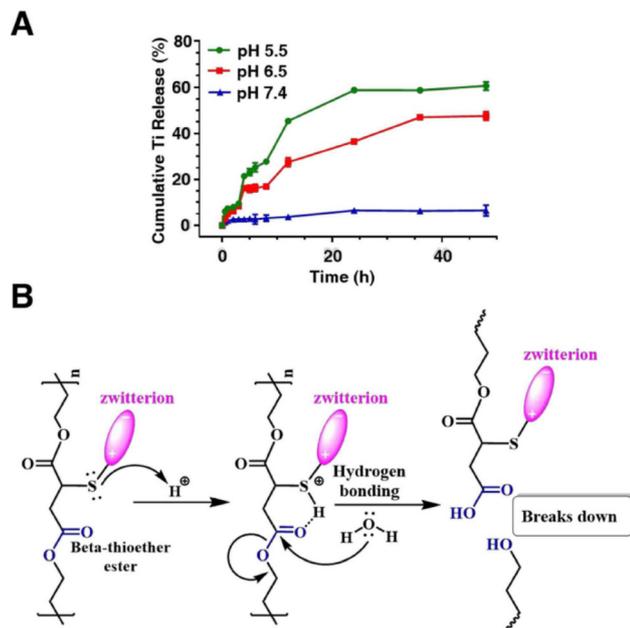
Fig. 5 (A) The drug release profiles of TiO_2 (expressed as a percentage of Ti release) in the TiO_{2-x}@TFPC nanocomposites in aqueous solutions at pH 7.4, pH 6.5, and pH 5.5. (B) The pH-responsive mechanism of the main chains on the polyester containing the beta-thioether ester structure in acidic media.
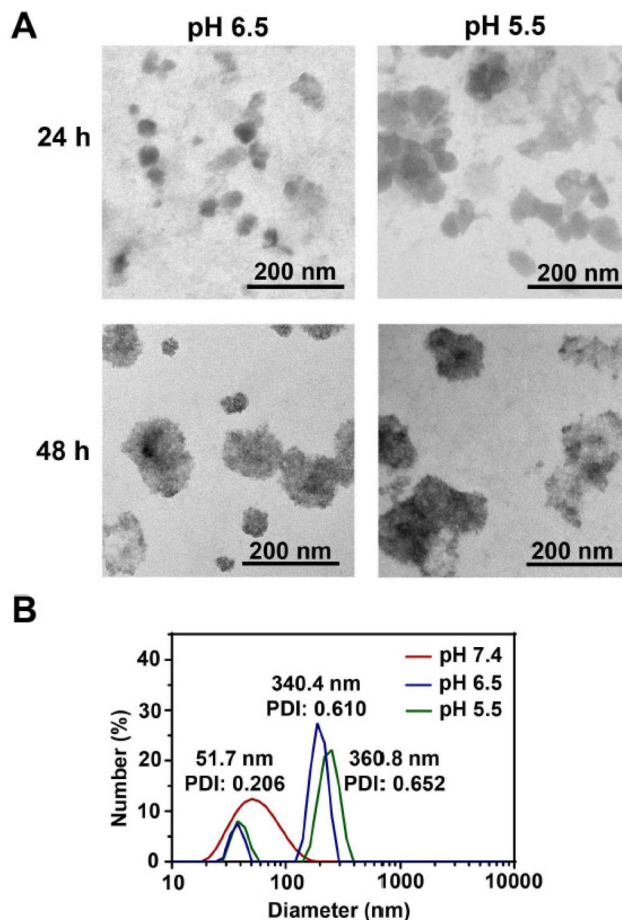

Fig. 6 (A) TEM images of zwitterionic porphyrin-based COP TFPC in buffer solutions at pH 6.5 or 5.5 for 24 h or 48 h. (B) Hydrodynamic size of TFPC in buffer solution at different pH values for 48 h measured by DLS.

were immersed at pH = 7.4 (PBS), the titanium drug was released at a slow rate with a low amount (6.43% over 48 h), indicating that the nanocomposites are relatively stable under physiological conditions, which can reduce the premature drug leakage. In contrast, the released amount of titanium drug at pH = 6.5 (acetate buffer solution) reached 47.6%. While the released amount of titanium drug at pH = 5.5 (acetate buffer solution) was the most, which reached 60.55%. Previously reported studies have shown that beta-thioesters are hydrolytically unstable in an acidic environment;[2,33] therefore, it is speculated that the mechanism of this release behavior was firstly the degradation of ester bonds between the PEG shell and the fumaryl group in the core of the zwitterionic porphyrin-based covalent organic polymer TFPC because of the effect of the adjacent unstable beta-thioesters (shown in Fig. 5B). Then the TiO_{2-x} nanoparticles that compounded through the steric stabilization effect of long polyethylene oxide side chains (2000 g mol^{-1}) on TFPC nanoparticles also leave following the degradation of PEG. The compounded effect of TiO_{2-x} nanoparticles is weakened. Finally, the TiO_{2-x} nanoparticles were released.

To demonstrate the presence of an acid-sensitive structure on the zwitterionic porphyrin-based COP for triggering biodegradation under an acid microenvironment, TEM and DLS detection experiments were tested. The TEM images and hydrodynamic sizes of TFPC in buffer solution at pH 6.5 or pH 5.5 for 24 h or 48 h are shown in Fig. 6. The TEM observation results (Fig. 6A) demonstrated the sizes and morphological change of TFPC after degradation. These changes of TFPC in sizes and morphologies were ascribed to the cleavage of ester

bonds between the PEG shell and the fumaryl group in the core of TFPC under the acid environment, detachment of PEG segments from the nanoparticle surface, an increase of the hydrophobicity and destabilization of the core of TFPC, which resulted in the formation of nanoparticle aggregates in the aqueous solution. When the environment is more acidic, the efficiency of the degradation of ester bonds between the PEG shell and the fumaryl group in the core is higher. As shown in Fig. 6B, comparing the TFPC nanoparticles dispersed in buffer solution at pH 7.4 and those at pH 6.5 for 48 h, the average sizes of nanoparticles increase dramatically from 51.7 nm to 340.4 nm. While in buffer solution at pH 5.5 for 48 h, the hydrodynamic size of TFPC is 360.8 nm. The size distributions of both TFPC nanoparticles in an acidic environment for 48 h show that these nano-systems exhibit a medium dispersion of the particle size. These experimental results all demonstrate the acid-sensitivity of zwitterionic porphyrin-based COP TFPC.

2.5 Determination of the generated $^1O_2$

The formation of singlet oxygen is the critical step in PDT. Because of the short survival time of $^1O_2$, it is necessary to find

a singlet oxygen capture agent to make it form a stable compound. 1,3-diphenylisobenzofuran (DPBF) can react with $^1O_2$ to produce the stable substrate 1,2-odibenzoylbenzene (Fig. S7A†). After capturing $^1O_2$ produced by a photosensitizer, the absorption intensity of DPBF will decrease at 350–470 nm. Therefore, the determination of the $^1O_2$ production capacity of the photosensitizer by the UV-visible spectrum of the capture agent DPBF can reflect the nano-system feasibility as a PDT drug.[48–50] The $^1O_2$ generated from TFPC or TiO$_{2-x}$@TFPC under 650 nm laser irradiation was determined by monitoring the absorption at 419 nm from the decomposition of DPBF in ethanol at 37 °C (Fig. 7). To explore the irradiation power and time dependent photodynamic activity, a series of TFPC ethanol solution samples were measured. With an increase in the irradiation power (from 200 to 300 mW) or time (different periods at 10, 15 and 30 min), the absorption of DPBF decreases (Fig. 7A and B), indicating that DPBF was oxidized by $^1O_2$ generated from the zwitterionic COP TFPC. Under laser irradiation at 300 mW for 30 min, DPBF decomposed by 8.5%, which is similar to the result of the previous report.[50] Moreover, the absorption of DPBF at 419 nm decreased obviously, when TFPC and DPBF ethanol solution was examined using a 630 nm laser (irradiation power density is 50 mW cm^{-2}, ~30 min) (Fig. S7B†). While with an increase in the irradiation time (~30 min) on the 650 nm laser irradiation power of 300 mW for TiO$_{2-x}$@TFPC, the absorption of DPBF decreased more obviously than that of plain TFPC at the same concentration (shown in Fig. 7B and C), which indicates that TiO$_{2-x}$@TFPC has a higher yield of $^1O_2$ compared to TFPC under laser irradiation. Fig. 7D shows that DPBF with

TiO$_{2-x}$@TFPC exhibits fast degradation under irradiation, and DPBF is decomposed by 82.6% in 30 min.

As compared with other representative porphyrin- or TiO$_2$-type nano-photosensitizers listed in Table S2,† the photodynamic effect of TiO$_{2-x}$@TFPC is outstanding. ROS production of TiO$_{2-x}$@TFPC is improved significantly as compared with the porphyrin-based nanoparticles TFP-NN.[50] The dosage of TiO$_{2-x}$@TFPC is much less than the upconversion nanoparticles containing TiO$_2$, and its ROS yield may be higher at the same laser irradiation time to some extent. Although the TSPP–TiO$_2$ nanocomposite contains the porphyrin ring and TiO$_2$, it is just used to treat rheumatoid arthritis, and its doses of lasers and photosensitizers are not clear.[51] In addition, compared with porphyrin-type single molecule photosensitizers, TiO$_{2-x}$@TFPC has a smaller dosage and a shorter irradiation time. These results and analyses indicate that TiO$_{2-x}$ as an additive can significantly improve the photodynamic effects of the zwitterionic COP TFPC.

2.6 Generation mechanism of $^1O_2$

The explanation for the above results may be that adding TiO$_{2-x}$ to TFPC can increase the light utilization efficiency and also improve the photoelectron production efficiency. The black anatase TiO$_{2-x}$ can be activated in the NIR region, which may be attributed to the donor–acceptor recombination and trapped electrons with free holes under weak excitation conditions.[52] The porphyrin group in TFPC is a p–π conjugated system composed of four pyrrole macrocycles. This structure can easily absorb visible light to produce electronic transitions, and in other words, the porphyrin groups absorb photons and switch from a low energy state to a high-energy excited triplet state. When the excited triplet state returns to the ground state of the porphyrin group, the excited triplet state can react with the triplet molecular oxygen ($^3O_2$), and energy transfer occurs followed by the formation of singlet oxygen $^1O_2$.[53] This process of light activated porphyrin groups in TFPC generating $^1O_2$ is shown in Scheme S2.† During laser irradiation, TFPC may decrease the recombination rate of the electron–hole pairs of TiO$_{2-x}$ by taking the electrons to generate $^1O_2$, thus increasing the half-life time of $^1O_2$ in TFPC.[16] The 650 nm laser irradiation can elevate the electrons of TiO$_{2-x}$@TFPC to a higher energy level (^{1}TiO$_{2-x}$@TFPC). Then, the long-lived triplet state of TiO$_{2-x}$@TFPC (^{3}TiO$_{2-x}$@TFPC) is transformed from the photo-excited ^{1}TiO$_{2-x}$@TFPC. Finally, $^1O_2$ is produced through the reaction between ^{3}TiO$_{2-x}$@TFPC and the surrounding ground state oxygen molecules $^3O_2$. Simultaneously, the cation radical of TFPC (TFPC$^+$) is formed and the electron (e$^-$) transfers from the excited TiO$_{2-x}$@TFPC nanocomposite to the CB of TiO$_{2-x}$ under irradiation. Then, the e$^-$ of the CB undergoes rapid re-oxidation to produce O$_2^{\bullet-}$ in the presence of $^3O_2$. Finally, the produced O$_2^{\bullet-}$ can be oxidized back to $^1O_2$. The schematic diagram of the $^1O_2$ generation of the TiO$_{2-x}$@TFPC system upon irradiation is shown in Scheme 2. Therefore, based on this mechanism, this composite strategy of the combination of TiO$_{2-x}$ with TFPC speeds
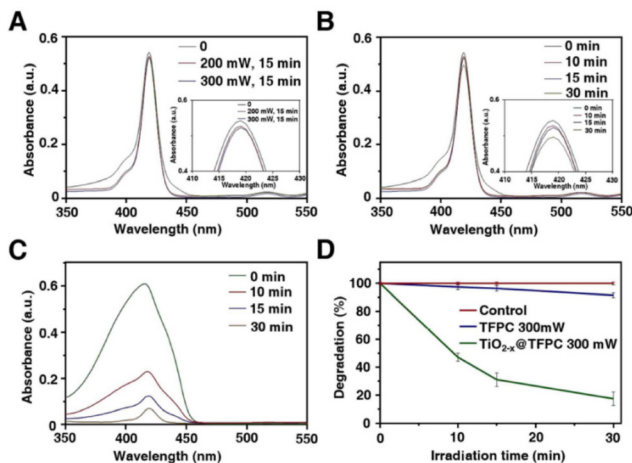

Fig. 7 Singlet oxygen mediated bleaching of the trapped molecule DPBF in the presence of TFPC (6.98 μg mL^{-1}) in ethanol solution, under irradiation with a 650 nm laser at 37 °C, (A) with diverse power densities for 15 min; (B) with different time points (power 300 mW). (C) Singlet oxygen mediated bleaching of the trapped molecule DPBF in the presence of TiO$_{2-x}$@TFPC (6.98 μg mL^{-1}) in ethanol solution, under irradiation with a 650 nm laser (power of 300 mW) at 37 °C. (D) Time-dependent degradation of DPBF with a mixed ethanol solution of TFPC or TiO$_{2-x}$@TFPC. The pure ethanol solution was used as a control. Error bars were based on the standard deviation of triplicate samples.
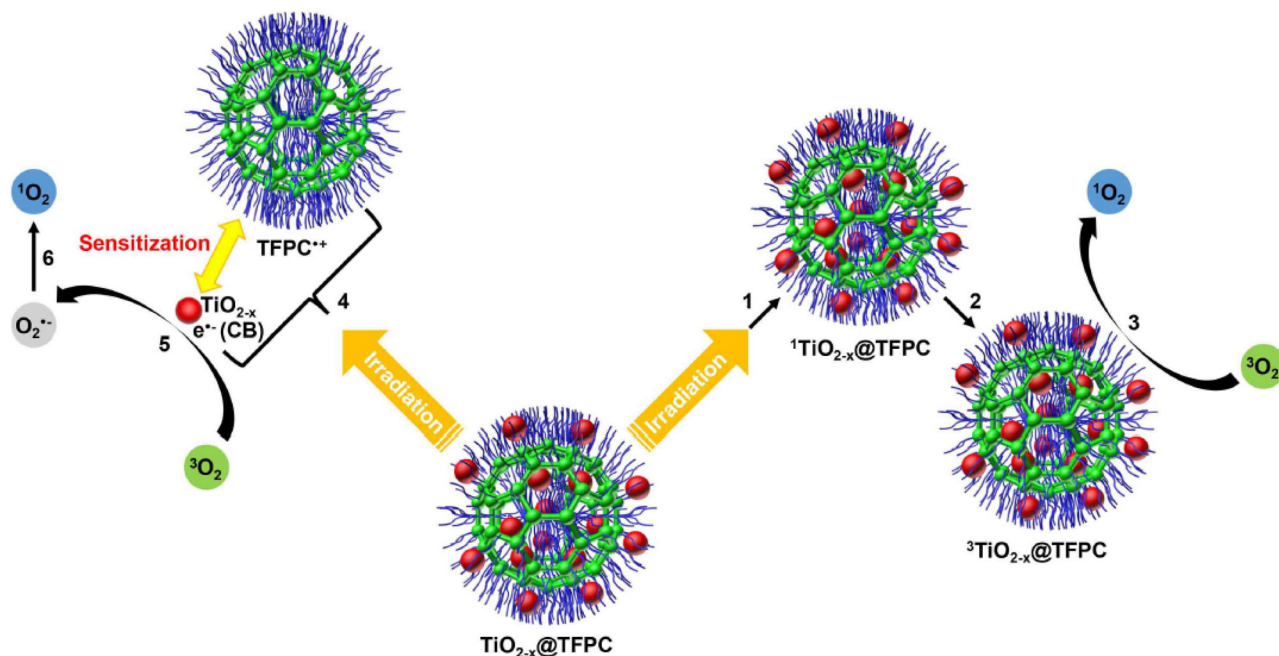
Scheme 2 The mechanisms of $^1O_2$ generation of the TiO_{2-x}@TFPC system by laser irradiation. (1: Absorption; 2: intersystem crossing; 3: energy transfer; 4: electron transfer between the excited TFPC and the conduction band (CB) of TiO_{2-x}; 5: re-oxidation; 6: oxidation of $O_2^{\bullet-}$ by the valence band hole (h^+).)

up the generation of $^1O_2$ and improves the photodynamic therapeutic activity.

2.7 *In vitro* photodynamic therapy and cytocompatibility

The photodynamic toxicity of TFPC nanoparticles and the TiO_{2-x}@TFPC nanocomposite was evaluated with drug-resistant liver cells (7404DDP) using the standard MTT assay *in vitro*. High concentrations of ROS can destroy mitochondria and DNA of cells and cause cell apoptosis.[54] The recently published work of the conjugated polymer for PDT is about a mitochondria-targeted nano-photosensitizer to generate a large amount of ROS in mitochondria, thus causing mitochondrial dysfunction and irreversible cell apoptosis.[55] Furthermore, applying a dual-step laser irradiation strategy to sequentially destroy singlet oxygen-responsive polymeric micelles and boost photodynamic cancer therapy can also cause cancer cell apoptosis effectively.[56] It can be seen in Fig. 8A that as the concentration of TFPC nanoparticles or TiO_{2-x}@TFPC nanocomposite aqueous solution increased, the viability of 7404DDP cells after cocultivation and irradiation treatment decreased, suggesting dose-dependent cytotoxicity. The TFPC nanoparticles and TiO_{2-x}@TFPC nanocomposites can be taken up by cancer cells, and then induce cancer cell death, due to the widely accepted enhanced permeability and retention (EPR) target effect and the photodynamic effect. The cells incubated with TiO_{2-x}@TFPC nanocomposites showed much lower cell viabilities than those treated with TFPC nanoparticles upon laser irradiation, indicating that the TiO_{2-x}@TFPC nanocomposites exhibited a higher drug-resistant liver cancer cell killing effect as compared with that of
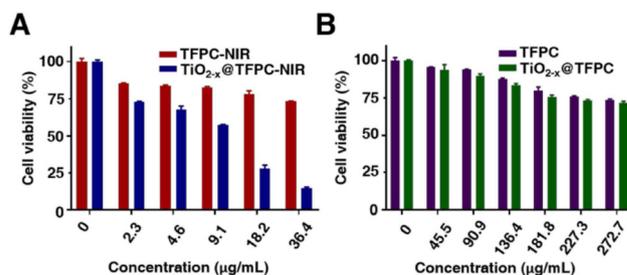

Fig. 8 *In vitro* MTT assays of nanoparticles and nanocomposites against drug-resistant cancer cells. Viability of 7404DDP cells with different TFPC nanoparticles and TiO_{2-x}@TFPC nanocomposite concentrations (A) in the presence of sequential NIR irradiation (650 nm, 300 mW, 15 min); (B) without laser irradiation.

TFPC nanoparticles. These results were consistent with their corresponding photodynamic effects as shown in Fig. 7. In the alternative photodynamic delivery system based on the zwitterionic porphyrin-based covalent organic polymer TFPC, the addition of black anatase TiO_{2-x} can improve the photodynamic toxicity toward drug-resistant cancer cells. The calculated IC_{50} (half maximal inhibitory concentration, which is the concentration needed to kill 50% of the 7404DDP cells) values of TiO_{2-x}@TFPC nanocomposites is 11.66 μg mL^{-1}. The low IC_{50} value of the TiO_{2-x}@TFPC nanocomposite suggests its strong photodynamic toxicity to drug-resistant liver cancer cells. Therefore, TiO_{2-x}@TFPC nanocomposites can act as a highly effective nano-photosensitizer for PDT treatment of drug-resistant liver cancer cells.

To verify the cytotoxicity of TFPC and TiO$_{2-x}$@TFPC in the absence of laser irradiation, the relative viability of 7404DDP cells cultured with TFPC nanoparticles or TiO$_{2-x}$@TFPC nanocomposites was also studied *via* the MTT assay, and the result is shown in Fig. 8B. The cell survival rate decreases slightly with an increase in the TFPC or TiO$_{2-x}$@TFPC concentration. However, it can be found from Fig. 8B that all the cell survival rates are above 71.9% when concentrations of TFPC nanoparticles or TiO$_{2-x}$@TFPC nanocomposites range from 45.5 to 272.7 μg mL^{-1}. These results demonstrate that the two zwitterionic porphyrin-based covalent organic polymer nanosystems both possess good cytocompatibility to drug-resistant cancer cells. The low toxicity and biocompatibility of TiO$_{2-x}$@TFPC may be due to the weak toxicity of TiO$_{2-x}$ in the dark[57] and the good cytocompatibility of PEG long chains and zwitterion L-cysteine side groups on the covalent organic polymer TFPC.

Therefore, various superior properties of the TiO$_{2-x}$@TFPC nanocomposite, such as acid-sensitivity, excellent photodynamic therapy capability for cancer and good cytocompatibility, make it a potential candidate for enhanced photodynamic therapy in biological systems. The strong fluorescence of the porphyrin ring in TFPC could be readily observed upon exposure to green light (500–550 nm),[51] which makes the nanocomposite TiO$_{2-x}$@TFPC a promising candidate for fluorescence imaging in cancer cells.

3. Conclusions

In summary, we have first successfully prepared an enhanced cancer photodynamic therapeutic nanocomposite agent, TiO$_{2-x}$@TFPC, for efficient target PDT treatment of cancer resistance. This agent combines the novel zwitterionic porphyrin polymer TFPC and the black anatase TiO$_{2-x}$. Under NIR laser irradiation, the TiO$_{2-x}$@TFPC nanocomposite can generate massive ROS to kill cancer cells, which is attributed to the photosensitive porphyrin groups in TFPC, the enormous oxygen vacancy sites of anatase TiO$_{2-x}$ nanocrystals, and the mutual sensitization of TFPC and TiO$_{2-x}$. The combination mechanism of TiO$_{2-x}$ and the zwitterionic porphyrin-based COP, and the mutual sensitization mechanism of TiO$_{2-x}$ and the zwitterionic porphyrin-based COP to produce ROS can guide the preparation of similar nanocomposite systems. The TiO$_{2-x}$@TFPC nanocomposite containing biocompatible TiO$_{2-x}$ and TFPC nanoparticles can ensure biosafety. Based on these results, this class of acid-sensitive TiO$_{2-x}$@TFPC nanocomposites provides a promising strategy for enhanced cancer photodynamic therapy with an accurate diagnosis by fluorescence imaging of further tumors and other diseases and for biomedical and clinical applications.

Conflicts of interest

There are no conflicts to declare.

References

1 R. L. Siegel, K. D. Miller and A. Jemal, *CA-Cancer J. Clin.*, 2018, **68**, 7.
2 J. X. Li, L. C. Zheng, H. H. Xiao, C. C. Li, S. H. Wu, Y. N. Xiao, J. J. Liu and B. Zhang, *Polym. Chem.*, 2019, **10**, 5353.
3 J. Wan, X. H. Zhang, D. S. Tang, T. Liu and H. H. Xiao, *Adv. Mater.*, 2023, e2209799, DOI: **10.1002/adma.202209799**.
4 Y. M. Spek, J. R. Kroep, R. A. E. M. Tollenaar and W. E. Meske, *Mol. Biol. Rep.*, 2020, **47**, 8169.
5 L. M. Xu, J. Liu, J. B. Xi, Q. L. Li, B. C. Chang, X. M. Duan, G. B. Wang, S. Wang, Z. Wang and L. Wang, *Small*, 2018, **14**, 1800785.
6 Y. X. Xing, T. Ding, Z. Q. Wang, L. C. Wang, H. D. Guan, J. Tang, D. Mo and J. X. Zhang, *ACS Appl. Mater. Interfaces*, 2019, **11**, 13945.
7 Q. X. Zhao, G. H. Liang, B. D. Guo, W. K. Wang, C. Yang, D. Chen, F. Y. Yang, H. H. Xiao and N. Z. Xing, *Adv. Sci.*, 2023, **10**, 2300175.
8 Z. N. Zhao, X. Zhang, C. Li and T. F. Chen, *Biomaterials*, 2019, **192**, 579.
9 J. L. Segura, M. J. Mancheno and F. Zamora, *Chem. Soc. Rev.*, 2016, **45**, 5635.
10 L. Y. Bai, S. Z. Fiona Phua, W. Q. Lim, A. Jana, Z. Luo, H. P. Tham, L. Z. Zhao, Q. Gao and Y. L. Zhao, *Chem. Commun.*, 2016, **52**, 4128.
11 V. S. Vyas, M. Vishwakarma, I. Moudrakovski, F. Haase, G. Savasci, C. Ochsenfeld, J. P. Spatz and B. V. Lotsch, *Adv. Mater.*, 2016, **28**, 8749.
12 Q. R. Fang, J. H. Wang, S. Gu, R. B. Kaspar, Z. B. Zhuang, J. Zheng, H. X. Guo, S. L. Qiu and Y. S. Yan, *J. Am. Chem. Soc.*, 2015, **137**, 8352.
13 J. Tan, N. Supawadee, K. Wei, K. Nawee, J. Guo and C. C. Wang, *Angew. Chem., Int. Ed.*, 2016, **55**, 13979.
14 H. R. Wang, W. W. Zhu, L. Z. Feng, Q. Chen, Y. Chao, Z. L. Dong and Z. Liu, *Nano Res.*, 2018, **11**, 3244.
15 H. R. Wang, W. W. Zhu, J. J. Liu, Z. L. Dong and Z. Liu, *ACS Appl. Mater. Interfaces*, 2018, **10**, 14475.
16 D. L. Tao, L. Z. Feng, Y. Chao, C. Liang, X. J. Song, H. R. Wang, K. Yang and Z. Liu, *Adv. Funct. Mater.*, 2018, **28**, 1804901.
17 E. Paszko, C. Ehrhardt, M. O. Senge, D. P. Kelleher and J. V. Reynolds, *Photodiagn. Photodyn. Ther.*, 2011, **8**, 14.
18 C. Nehate, A. A. Moothedathu Raynold, V. Haridas and V. Koul, *Biomacromolecules*, 2018, **19**, 2549.
19 Y. Qin, L. Sun, X. X. Li, Q. Q. Cao, H. Wang, X. F. Tang and L. Ye, *J. Mater. Chem.*, 2011, **21**, 18003.

20 V. Etacheri, C. Di Valentin, J. Schneider, D. W. Bahnemann and S. C. Pillai, *J. Photochem. Photobiol., C*, 2015, **25**, 1.

21 T. Hasegawa, A. B. Béléké and M. Mizuhata, *J. Power Sources*, 2013, **233**, 148.

22 J. Wang, Z. Peng, J. Huang, Y. Zhang, X. Zhang, Y. Wang, Y. Fu, W. Li, J. Chen and K. Chen, *Sol. Energy Mater. Sol. Cells*, 2023, **257**, 112348.

23 P. Rajaram, A. R. Jeice and K. Jayakumar, *Surf. Interfaces*, 2023, **39**, 102912.

24 Z. Hu, Y. D. Huang, S. F. Sun, W. C. Guan, Y. H. Yao, P. Y. Tang and C. Y. Li, *Carbon*, 2012, **50**, 994.

25 H. J. Zhang, X. L. Zhu, Y. D. Ji, X. J. Jiao, Q. Q. Chen, L. Hou, H. L. Zhang and Z. Z. Zhang, *J. Mater. Chem. B*, 2015, **3**, 6310.

26 Z. Y. Hou, Y. X. Zhang, K. R. Deng, Y. Y. Chen, X. J. Li, X. R. Deng, Z. Y. Cheng, H. Z. Lian, C. X. Li and J. Lin, *ACS Nano*, 2015, **9**, 2584.

27 L. Y. Zeng, Y. W. Pan, Y. Tian, X. Wang, W. Z. Ren, S. J. Wang, G. M. Lu and A. G. Wu, *Biomaterials*, 2015, **57**, 93.

28 J. Zhou, P. Luo, C. Sun, L. C. Meng, W. R. Ye, S. S. Chen and B. Du, *Nanoscale*, 2017, **9**, 4244.

29 S. G. Ullattil and P. Periyat, *J. Mater. Chem. A*, 2016, **4**, 5854.

30 W. Z. Ren, Y. Yan, L. Y. Zeng, Z. Z. Shi, A. Gong, P. Schaaf, D. Wang, J. S. Zhao, B. B. Zou, H. S. Yu, G. Chen, E. M. B. Brown and A. G. Wu, *Adv. Healthcare Mater.*, 2015, **4**, 1526.

31 C. Y. Fan, C. Chen, J. Wang, X. X. Fu, Z. M. Ren, G. D. Qian and Z. Y. Wang, *Sci. Rep.*, 2015, **5**, 11712.

32 M. Niederberger and G. Garnweitner, *Chem. – Eur. J.*, 2006, **12**, 7282.

33 R. G. Schoenmakers, P. Wetering, D. L. Elbert and J. A. Hubbell, *J. Controlled Release*, 2004, **95**, 291.

34 V. V. Atuchin, *J. Mater. Chem. A*, 2017, **5**, 426.

35 R. Ren, Z. H. Wen, S. M. Cui, Y. Hou, X. R. Guo and J. H. Chen, *Sci. Rep.*, 2015, **5**, 10714.

36 M. Y. Xing, J. L. Zhang, F. Chen and B. Z. Tian, *Chem. Commun.*, 2011, **47**, 4947.

37 P. V. R. K. Ramacharyulu, D. B. Nimbalkar, J. P. Kumar, G. K. Prasad and S. C. Ke, *RSC Adv.*, 2015, **5**, 37096.

38 X. B. Chen, L. Liu, Y. P. Yu and S. S. Mao, *Science*, 2011, **331**, 746.

39 A. Naldoni, M. Allieta, S. Santangelo, M. Marelli, F. Fabbri, S. Cappelli, C. L. Bianchi, R. Psaro and V. D. Santo, *J. Am. Chem. Soc.*, 2012, **134**, 7600.

40 U. Zavyalova, B. Nigrovski, K. Pollok, F. Langenhorst, B. Müller, P. Scholz and B. Ondruschka, *Appl. Catal., B*, 2008, **83**, 221.

41 X. Chen, D. X. Zhao, K. W. Liu, C. R. Wang, L. Liu, B. H. Li, Z. Z. Zhang and D. S. Shen, *ACS Appl. Mater. Interfaces*, 2015, **7**, 16070.

42 V. Etacheri, C. Di Valentin, J. Schneider, D. W. Bahnemann and S. C. Pillai, *J. Photochem. Photobiol., C*, 2015, **25**, 1.

43 S. G. Ullattil and P. Periyat, *Nanoscale*, 2015, **7**, 19184.

44 S. Koch, M. Kessler, K. Mandel, S. Dembski, K. Heuzé and S. Hackenberg, *Colloids Surf., B*, 2016, **143**, 7.

45 E. Csapó, R. Patakfalvi, V. Hornok, L. T. Tóth, Á. Sipos, A. Szalai, M. Csete and I. Dékány, *Colloids Surf., B*, 2012, **98**, 43.

46 A. Lalloz, M. Bolzinger, J. Faivre, P. Latreille, A. G. Ac, C. Rakotovao, J. Rabanel, P. Hildgen, X. Banquy and S. Briançon, *Int. J. Pharm.*, 2018, **553**, 120.

47 R. Gref, G. Miralles and E. Dellacherie, *Polym. Int.*, 1999, **48**, 251.

48 R. C. Lv, P. P. Yang, F. He, S. L. Gai, G. X. Yang, Y. L. Dai, Z. Y. Hou and J. Lin, *Biomaterials*, 2015, **63**, 115.

49 S. I. Turan, D. Yildiz, A. Turksoy, G. Gunaydin and E. Akkaya, *Angew. Chem., Int. Ed.*, 2016, **55**, 2875.

50 R. Xia, X. H. Zheng, X. L. Hu, S. Liu and Z. G. Xie, *ACS Appl. Mater. Interfaces*, 2019, **11**, 5782.

51 C. Q. Zhao, F. U. Rehman, H. Jiang, M. Selke, X. M. Wang and C.-Y. Liu, *Sci. China: Chem.*, 2016, **59**, 637.

52 X. L. Wang, Z. C. Feng, J. Y. Shi, G. Q. Jia, S. Shen, J. Zhou and C. Li, *Phys. Chem. Chem. Phys.*, 2010, **12**, 7083.

53 K. R. Weishaupt, C. J. Gomer and T. J. Gougherty, *Cancer Res.*, 1976, **36**, 2326.

54 H. J. Zhang, Y. F. Shan and L. J. Dong, *J. Biomed. Nanotechnol.*, 2014, **10**, 1450.

55 L. Yang, P. Gao, Y. Huang, X. Lu, Q. Chang, W. Pan, N. Li and B. Tang, *Chin. Chem. Lett.*, 2019, **30**, 1293.

56 K. Deng, H. Yu, J.-M. Li, K.-H. Li, H.-Y. Zhao, M. Ke and S.-W. Huang, *Biomaterials*, 2021, **275**, 120959.

57 Y. Ding, L. Zhou, X. Chen, Q. Wu, Z. Y. Song, S. H. Wei, J. H. Zhou and J. Shen, *Int. J. Pharm.*, 2016, **498**, 335.